IEEE Access
Multidisciplinary | Rapid Review | Open Access Journal

Received November 18, 2019, accepted December 15, 2019, date of publication December 23, 2019,
date of current version January 2, 2020.

Digital Object Identifier 10.1109/ACCESS.2019.2961691

Chipless RFID Tag for Touch Event Sensing and Localization

LAIBA SHAHID[1], HUMAYUN SHAHID[1], (Member, IEEE), MUHAMMAD ALI RIAZ[1], (Member, IEEE), SYEDA IFFAT NAQVI[1], (Member, IEEE), MUHAMMAD JAMIL KHAN[1], (Member, IEEE), MANSOOR SHAUKAT KHAN[2], YASAR AMIN[1], (Senior Member, IEEE), AND JONATHAN LOO[3], (Member, IEEE)

[1]ACTSENA Research Group, University of Engineering and Technology, Taxila 47050, Pakistan
[2]Mathematics Department, COMSATS University, Islamabad 45550, Pakistan
[3]School of Computing and Engineering, University of West London, London W5 5RF, U.K.

Corresponding author: Humayun Shahid (humayun.shahid@uettaxila.edu.pk)

This work was supported in part by the Higher Education Commission (HEC) of Pakistan through the Technology Development Fund under Grant TDF-67/2017, in part by the Department of Electronic Systems, Royal Institute of Technology (KTH), Sweden, and in part by the ASR&TD-UETT Faculty Research Grant.

ABSTRACT A novel Radio Frequency Identification (RFID) based sensor supporting touch detection and localization features is proposed in this work. The formulated sensor leverages chipless variant of RFID technology for the design of a passive fully-printable frequency domain-based sensor-incorporated tag. The sensor is composed of square resonators arranged in a peculiar fashion laid down across a 3 × 2 grid. The proposed sensor incorporated-tag readily keeps track of human-digit position, allowing for tracking of finger-swipes which, in turn, can potentially be used for recognition of unlock patterns and security codes. Performance of the sensor is analyzed using its Radar Cross Section (RCS) response observable in the spectral domain. Each constituent resonant-element making up the sensor resonates at a single frequency represented by a distinct dip in the RCS response. The spectral dip drifts well outside of its allocated band upon occurrence of a touch event. A functional prototype of the sensor tag is fabricated on a 0.508 mm thick Rogers RT/Duroid® 5880 laminate is scrutinized of its electromagnetic performance. The sensor possesses a compact physical footprint equal to 45 mm × 55 mm. The obtained results solidify the suitability of the proposed sensor for deployment in secure access control settings prevalent in smart cities and connected home applications.

INDEX TERMS Chipless tag, radio frequency identification (RFID), RFID sensor, radar cross-section (RCS), touch sensor.

I. INTRODUCTION

Modern-day research efforts are extensively focused on developing low-cost solutions for wireless sensing due to a pronounced shift towards pervasive computing. Wireless technologies, including ZigBee, Bluetooth, and wireless local area networks (WLANs), inherently require relatively higher amount of power for their operation, and come with significant circuital complexity. This contributes to both a higher overall system cost and a limited device lifespan. Radio Frequency Identification (RFID) technology provides a cost-effective and long-term solution in this regard [1]. RFID tags can be active, semi-passive and passive. Active and semi-passive tags require batteries for their operation whereas passive tags are essentially battery-less in their construction. Both semi-passive and passive tags operate on the principle of backscattering, and energization of the tag itself depends upon the electromagnetic waves originating from the reader. The imping waves are backscattered towards the reader unit along with the stored data. This makes such tags a preferred choice for applications falling under the scope of Internet of Things (IoT) paradigm [2]. Passive tags can either be chip-based or chipless. Sensing is achieved in chip-based tags by incorporating the sensor's data within the integrated circuit which remains an integral component of the tag. In terms of cost, the dedicated silicon chip is, by far,

The associate editor coordinating the review of this manuscript and approving it for publication was Qiquan Qiao.

the most expensive component within a sensor-incorporated RFID tag. Inclusion of the chip makes the solution unfeasible for mass-market adoption. Chipless RFID tags, on the other hand, neither have an associated threshold activation power rating, nor the requirement of a dedicated application specific integrated circuit (ASIC). This opens up the possibility of developing chipless sensors and systems that allow for wireless sensing and offer both reliability and cost-effectiveness [3].

Implementation of various sensors using chipless RFID technology has been explored. Humidity sensors, temperature sensors, gas-emission sensors, and displacement sensors etc. are the fields which are more have been investigated in detail. Multiple techniques have been employed for realizing the said sensors. Artificial Impedance Surfaces [4], FSS-based resonators fabricated on cardboard and Mitsubishi paper [5], [6], inkjet-printed sensors on paper substrate [7] and silver nanotubes-based sensors [8] are some of the approaches that have been adapted for sensing of humidity. Chipless RFID sensors have also been used for sensing of temperature. Dielectric substrates sensitive to changes in temperature have been used extensively in design of sensor-incorporated chipless data encoding circuits that are responsive to changes in temperature [9]–[11]. A chipless wireless temperature-threshold sensor has been implemented in [12] by integration of several slot resonators in a multi-bit C-shaped scatterers. For detection of gaseous emissions, carbon nanotube-based resonant structures have been proposed that find utility in environmental monitoring [13].

Sensors for human touch detection have also been presented. Such sensors, for most part, are chip-based and make use of a dedicated silicon chip for their operation. The presence of a dedicated integrated circuit adds up significantly in the overall fabrication cost [14]. Touch event sensors are typically based upon physical interaction between the sensor-incorporated tag and the end-user. Essentially, the tags operate by detecting touch events through a noticeable alteration in the electromagnetic response [15]–[17]. Albeit in early stages, an approach based on chipless RFID technology has recently been ideated that relies on modification of the tag's scattering parameters upon occurrence of single-touch event [18].

In this work, we propose a chipless data encoding circuit that has been repurposed [19] for detection and localization of human touch events. The proposed sensor-incorporated tag is capable of detecting instances of single-touch events at six distinct locations in full-wireless mode. The formulated sensor tag functions without having to rely on a dedicated silicon chip for its operation, establishing itself as a cost-effective competitor when stacked against chip-based alternatives. The proposed tag is provisioned with a ground plane, enabling placement of both the transmit and the reader antenna on the same side. This facilitates deployment of the proposed sensor tag in typical user-authentication scenarios. The proposed tag operates by recording disappearance of resonant dips in the spectral response. The formulated tag performs sensing and localization by keeping track of presence and absence of corresponding resonant dips in the Radar Cross-Section (RCS) response for both the touched and untouched state. The proposed tag offers a clear advantage due to its cost-effectiveness and reduced circuital complexity, making it suitable for conventional as well as wearable Internet of Things (IoT) applications.

II. CHIPLESS RFID SENSOR DESIGNING

A. OPERATING PRINCIPLE

The proposed sensor tag has been developed to function in the spectral domain. The design is composed of resonant elements that function similar to a frequency selective surface (FSS), except that in this case there is no repetition of single unit cell. The resulting surface is capable of absorbing certain wavelengths of incident electromagnetic waves while scattering others back towards the source. This phenomenon of selective absorption and reflection leads to appearance of distinct spectral notches in the RCS response of the sensor-incorporated chipless RFID tag.

The proposed sensor-incorporated tag, inspired from [18], operates in the far-field [20], where the read-range can be determined using Friis transmission equation [21].When a resonant element is impinged upon by an interrogating electromagnetic wave at a particular frequency, an atypical surface current distribution is observed across the corresponding geometrical structure. Depicted in Fig. 1, the peculiar distribution is characterized by presence of minimal current density towards the top and bottom vertices of the structure. The minimal current density indicates the presence of inductive characteristics. Four corners of the geometric structure, on the other hand, are home to maximal distribution of surface current, signifying presence of capacitive effects.

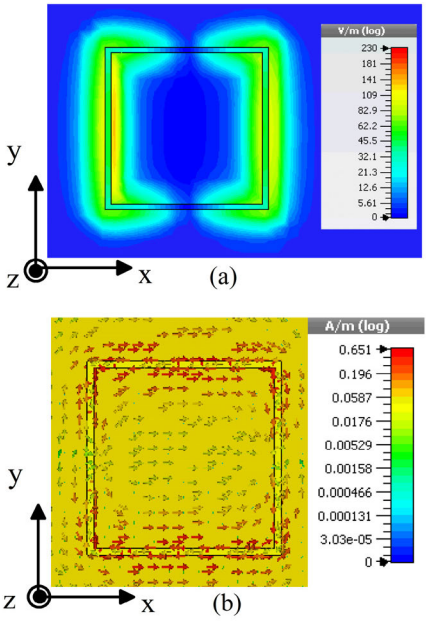

FIGURE 1. (a) Electric field distribution (b) Surface current distribution.

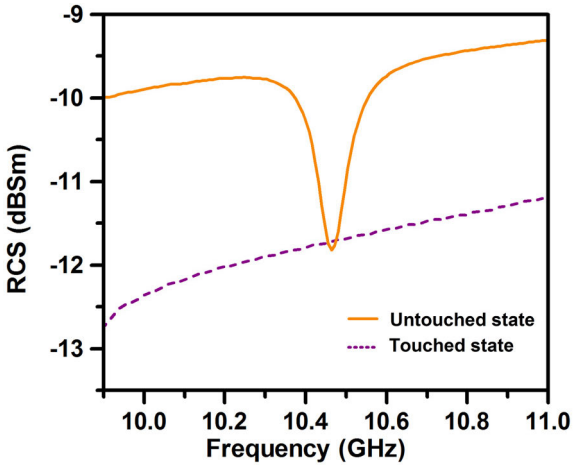

FIGURE 2. Operating principle of the tag. The curve in orange shows the RCS response in the untouched state, whereas the one in purple depicts the same in case of a touch event.

The concurrent existence of inductive and capacitive characteristics distributed across a single geometric structure results in generation of a pronounced spectral dip [22]. The spectral dip is readily observable in the RCS response of the resonant element as has been shown in Fig. 2, plotted with a solid line. When the human digit comes in direct contact with a resonant element, the corresponding value of capacitance undergoes a significant change, disrupting the peculiar current distribution across the geometrical structure. This disruption, in turn, leads to a significant alteration in the effective permittivity of the sensor tag. This causes the corresponding spectral dip to undergo a diminishment from the band of interest, as has been plotted in Fig. 2, using a dotted line.

B. PRELIMINARY GUIDELINES

Interacting with cellphone touchscreens has become second nature for majority of individuals. It is for this very reason that the design of the proposed chipless tactile sensor is subjected to constraints put forward in the human-interface guidelines publicized by Apple® [23] and Google® [24]. The two device makers have captured a sizable portion of the global smartphone market share. For devices powered by the iOS platform, Apple® has specified a minimum tappable area as being equal to 44pt × 44pt. The measure corresponds to physical dimensions that equal 15.5 mm × 15.5 mm. Likewise, design guidelines available for Google's Android® operating system recommend that the target touch size to be equal to at least 48dp × 48dp. This translates to physical dimensions that equal 9 mm × 9 mm. In addition, the standard also suggests a minimum spacing of 8dp between touch targets placed in vicinity of one another.

Taking into consideration the geometrical constraints put forward in the above-mentioned human interaction guidelines, the proposed tag has been designed to include six resonators that have been positioned meticulously across a 3 × 2 grid, as shown in Fig. 3 (a). The sensor-incorporated tag follows a layout defined by two horizontal and three vertical segments., A resonator has been realized in the middle of each of the six resulting bounding boxes. While each resonant element bears unique physical dimensions, the side-width is kept at 0.4 mm for all resonant elements that make up the proposed sensor tag. As detailed in Fig. 3 (b), each resonant element gives rise to a distinct peak in the RCS response of the proposed sensor at a specific value of frequency. Resonant elements numbered as 1, 2, 3, 4, 5, 6 have been known to resonate at frequencies specified by 10.49 GHz, 9.46 GHz, 8.22 GHz, 6.73 GHz, 5.60 GHz, and 4.97 GHz, respectively. Dimensions of the tag are optimized to be 45 × 55 mm^2 and the design is materialized on Rogers RT/Duroid®5880 substrate having a dielectric constant equal to 2.2 and a thickness equal to 0.508 mm. The tag is provisioned with a metallic ground plane which not only enhances the quality factor of the spectral dips but also extends the scope of the sensor tag by making the same amenable for applications where on-metal deployment is highly sought after appropriate geometric optimization. Excitation of the tag is performed using a horizontally polarized electromagnetic wave. Simulated results have been obtained using state-of-the-art, full-wave electromagnetic simulation software Computer Simulation Technology® MICROWAVE STUDIO® (CST® MWS®).

C. FINGER MODELLING

For performing computer-aided analysis of the proposed tag's resonant behavior in response to a touch event, a three-layered cylindrical finger model has been employed. Fig. 4 depicts the constituent layers making up the cylindrical finger model. The electromagnetic characteristics of the layers making up the human digit model have been extracted from studies carried out earlier on reported in [25]–[27] and have been summarized in Table 1. Keeping in view the results presented in [28], radius of the finger model is kept as 7.75 mm. As soon as the finger comes in direct contact with any of the resonant elements, the electrical permittivity of the resonator undergoes an alteration. The phenomenon leads to disappearance of the corresponding spectral dip associated with the resonant structure where a touch event has been registered. As an outcome, the number of resonant peaks in the RCS response decreases from six to five. The decrease in the number of resonant peaks indicates that a touch event has indeed taken place, validating the touch-detection capability of the proposed sensor tag.

TABLE 1. Human fingertip layer elements.

Element Layer	Permitivity	Bulk Conductivity (S/m)	Bulk density (Kg/m^3)	Thickness (mm)
Skin	38	1.464	1100	2
Fat	5.24	0.104	1100	4
Bone	15.0087	0.586	1850	3.4

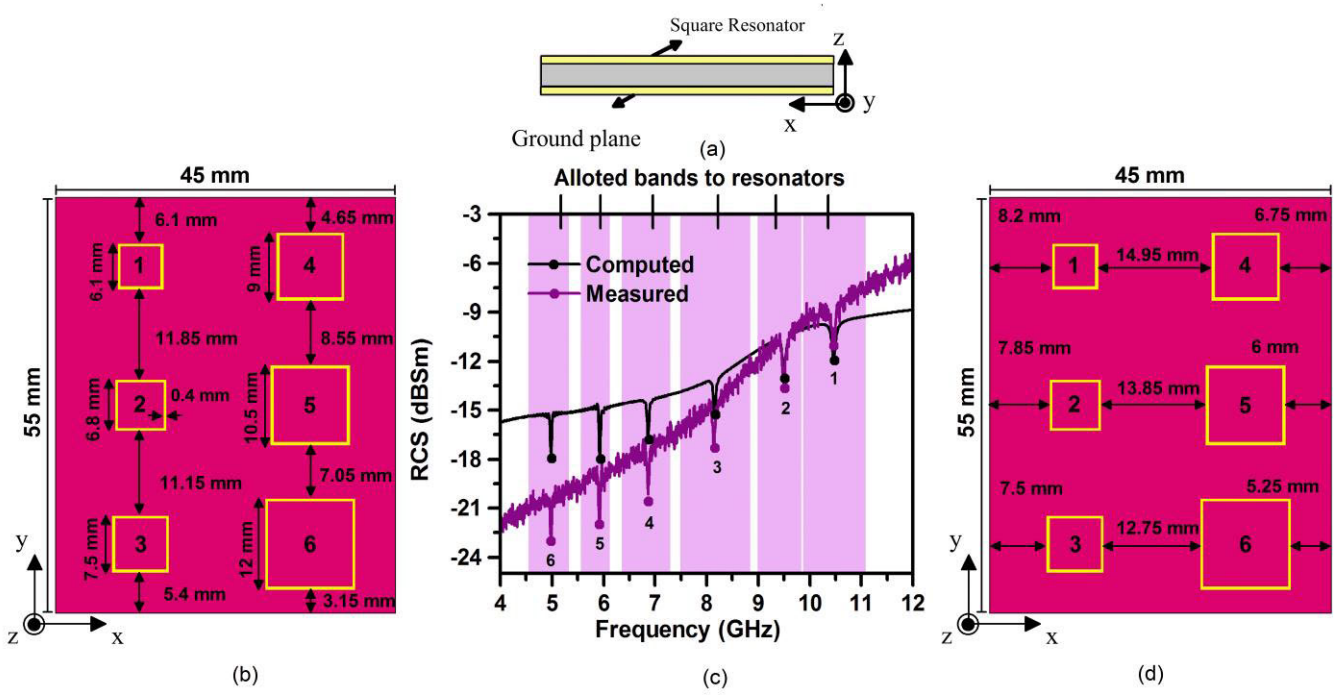

FIGURE 3. (a) Lateral-view of the tag depicting three layers (b) Resonator dimensions and inter-resonator spacing along y-axis (c) Sensor-tag response in untouched state (d) Inter-resonator spacing along x-direction.

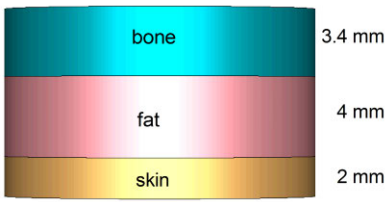

FIGURE 4. Finger layer model.

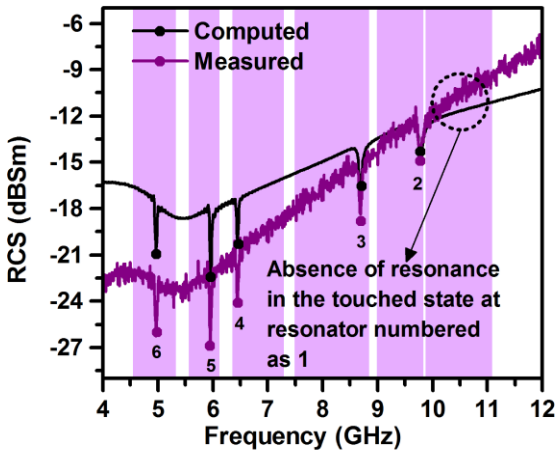

FIGURE 5. Obtained response while finger location at Resonator 1.

Moreover, the exact position where the human digit has landed on the sensor's surface can also be determined using the proposed design. As a first step, the process involves identifying the spectral dip that has undergone diminishment. The information is then used in the second step to determine the corresponding resonant element where the touch event has taken place is most likely to have taken place. The approach allows for localization of touch events and can also be used to pin-point the resonant element where tactile contact has precisely been established, paving the way for implementation of various gesture-related and security-centric applications.

III. RESULTS AND DISCUSSION

Geometrical dimensions of the proposed tag have been optimized parametrically using state-of-the-art full-wave electromagnetic simulation tool CST® MWS®. Since the proposed structure itself is made up of six resonant elements, the optimization process takes into account the response obtained individual resonator in response to a touch event taking place at a resonator itself as well as in its vicinity. The process of optimization leads to assignment of specific frequency bands to each of the constituent resonant elements. The spectral allocation has been summarized in Table 2.

This assignment of frequency bands enables detection and is imperative for imparting touch-detection and localization capabilities to the proposed sensor-incorporated tag. RCS response of the proposed sensor-incorporated tag is studied while positioning finger one-by-one on each of the constituent resonant elements. Fig. 5 depicts the measured and computed response of resonant element 1 upon human

TABLE 2. Assigned frequency bands for individual resonators.

Resonator no.	Alloted bands (GHz)	Spectral Width (GHz)
1	9.85 – 11	1.15
2	9 – 9.85	0.85
3	7.6 – 8.8	1.2
4	6.4 – 7.3	0.9
5	5.6 – 6.1	0.5
6	4.5 – 5.3	0.8

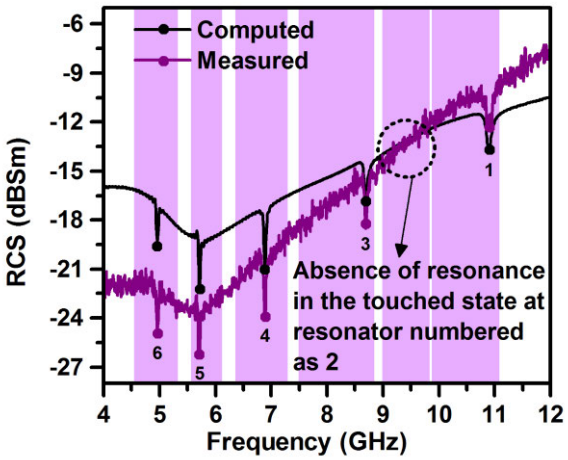

FIGURE 6. Obtained response while finger location at Resonator 2.

finger contact. Presence of the finger alters the electromagnetic response for resonator 1 in such a way the spectral dip originally present at 10.49 GHz ceases to exist. A decrease in the total number of resonances from six to five indicates that a touch event has taken place. Moreover, the absence of a resonant dip in the allocated range from 9.85 GHz – 11 GHz signifies that a touch event has taken place on the sensor surface specified by resonant element 1. In this way, detection and localization capabilities for single-touch events sported by the proposed sensor are validated.

Moving forward, human digit is now positioned such that it lands at resonant element numbered as 2. In absence of finger, the frequency associated with it is 9.46 GHz. As illustrated in Fig. 6, the computationally-determined as well as the measured response depicts absence of a resonant dip within the designated spectral band spanning from 9 GHz – 9.85 GHz upon occurrence of a touch event. Again, with the total number of resonant dips reduced to five, and with a readily-identifiable presence of a single spectral dips in other spectral bands other than in the 9 GHz – 9.85 GHz region, the operational capability of the proposed tag becomes evident.

Similarly, resonant element 3, having physical dimensions of 7.5 mm × 7.5 mm resonates at 8.22 GHz in the untouched state. When a human digit comes in direct contact with the surface of the sensor at the location specified by resonator 3, the corresponding spectral dip at 8.22 GHz disappears from

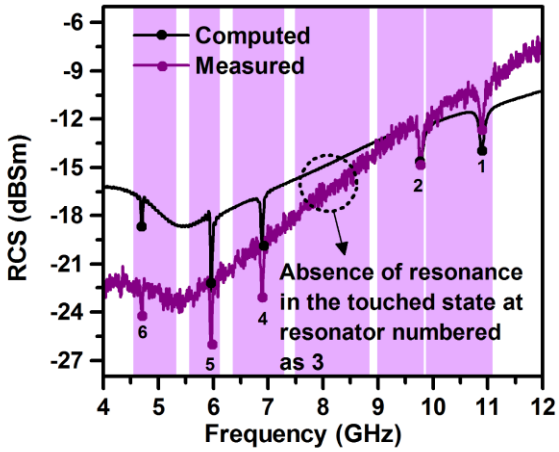

FIGURE 7. Obtained response while finger location at Resonator 3.

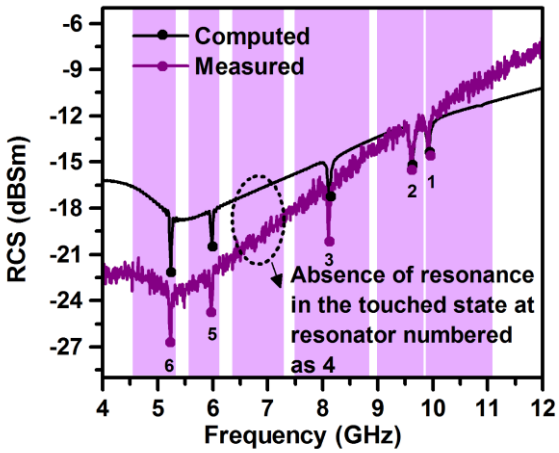

FIGURE 8. Obtained response while finger location at Resonator 4.

its designated spectral neighborhood. Once again, as an outcome of the touch event, the number of spectral dips undergoes a decrement by one reducing the total to five. Fig. 7 overlays the computed and measured results over the same axis. The graph indicates that the resonant dip that was previously there in the allocated spectral band from 7.6 GHz – 8.8 GHz no longer exists. It is worth noting that resonant dips situated in other spectral neighborhoods remain unaffected.

The RCS response obtained when a touch event takes place at the resonant element labelled 4 is shown in Fig. 8. Resonant element 4, in the untouched state, resonates at 6.73 GHz. In the wake of a touch event, the resonant dip associated with resonant element 4 goes well outside of the designated spectral band of 6.4 GHz – 7.3 GHz, whereas the others remain well within their allocated spectral bounds. This indicates occurrence of a touch event which can also readily be localized.

For the element designated as resonator 5, the corresponding spectral dip is obtained at 5.60 GHz in the untouched state. Upon being touched, the resonant dip drifts well outside of its designated band i.e. 5.6 GHz – 6.1 GHz. It is worth

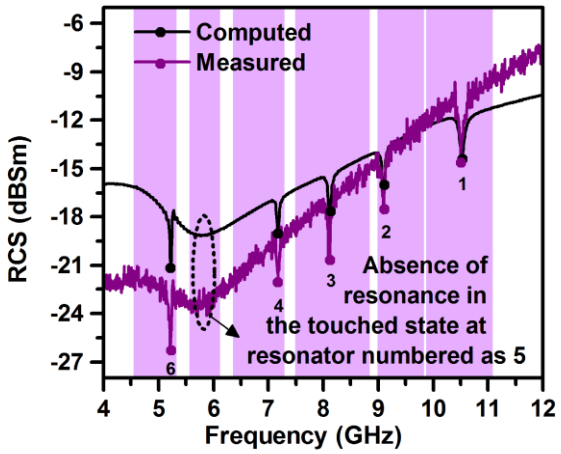

FIGURE 9. Obtained response while finger location at Resonator 5.

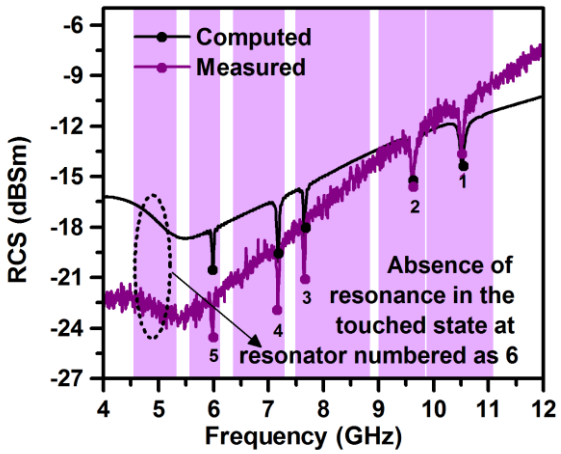

FIGURE 10. Obtained response while finger location at Resonator 6.

noting that all other spectral dips remain within their designated frequency bands. A decrement in the overall dip count from six to five as well as the nonexistence of the same in the above-mentioned spectral neighborhood signifies that a touch event has occurred that be easily traced back to resonator 5. Fig. 9 presents the RCS response upon occurrence of a touch event.

The RCS response when a touch event has taken place at resonator 6 is presented in Fig. 10. Positioning the human digit on resonant element 6 results in the corresponding resonant dip, which had otherwise been observable at 4.97 GHz, to drift outside of its allocated spectral band ranging from 4.5 GHz – 5.3 GHz. On the other hand, resonant dips remain well within the spectral bands that have originally been allocated to them.

A number of prototypes of the proposed sensor-incorporated tag have been fabricated and scrutinized for their experimental performance. Well-known experimental arrangement for far-field RCS measurement has been utilized for making the measurements. The setup for experimental measurements comprises of a pair of identical horn-antennae, multiple prototypes of the sensor-incorporated tag under

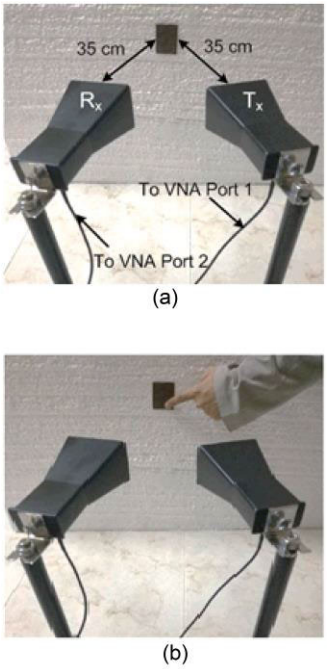

FIGURE 11. Setup for obtaining experimental results for the sensor-tag placed on Styrofoam (a) for the untouched state (b) for a single-touch event.

test, and test equipment vector network analyzer (VNA) R&S® ZVL-13. A pictorial depiction of the testbench for measurement of experimental results has been provided in the Fig.11.

One of the horn antenna acts as the transmit antenna and other one acts as the receiving antenna. The transmit antenna is connected to port 1 whereas the receiving antenna is connected to port 2 of the VNA to analyze the S21 parameter. During the measurement process, transmit power equal to 0 dBm is used over the frequency range spanning from 4.5 to 11 GHz. Once S_{21} has been obtained, Equation 1 shown below is used to estimate the value of RCS. In Equation 1, σ^{ref} represents the RCS for an object that is predetermined, for instance a plain rectangular metal plate. S_{21}-tag is the response obtained in presence of the chipless RFID tag. The procedure for RCS determination also incorporates within itself the part where calibration comes in because of S_{21}-isolation that has been calculated in the absence of chipless RFID tag. Doing so does away with unwanted environmental effects that may plague the measured RCS

$$\sigma^{tag} = \left[\frac{S_{21}^{tag} - S_{21}^{isolation}}{S_{21}^{ref} - S_{21}^{isolation}}\right]^2 \sigma^{ref} \quad (1)$$

During the measurement phase, the distance between the floor and the proposed sensor-incorporated chipless RFID tag is an important consideration that needs to be taken account. While the method of carrying out the RCS measurement itself does away with environmental effects to a great extent, the electromagnetic waves being reflected off

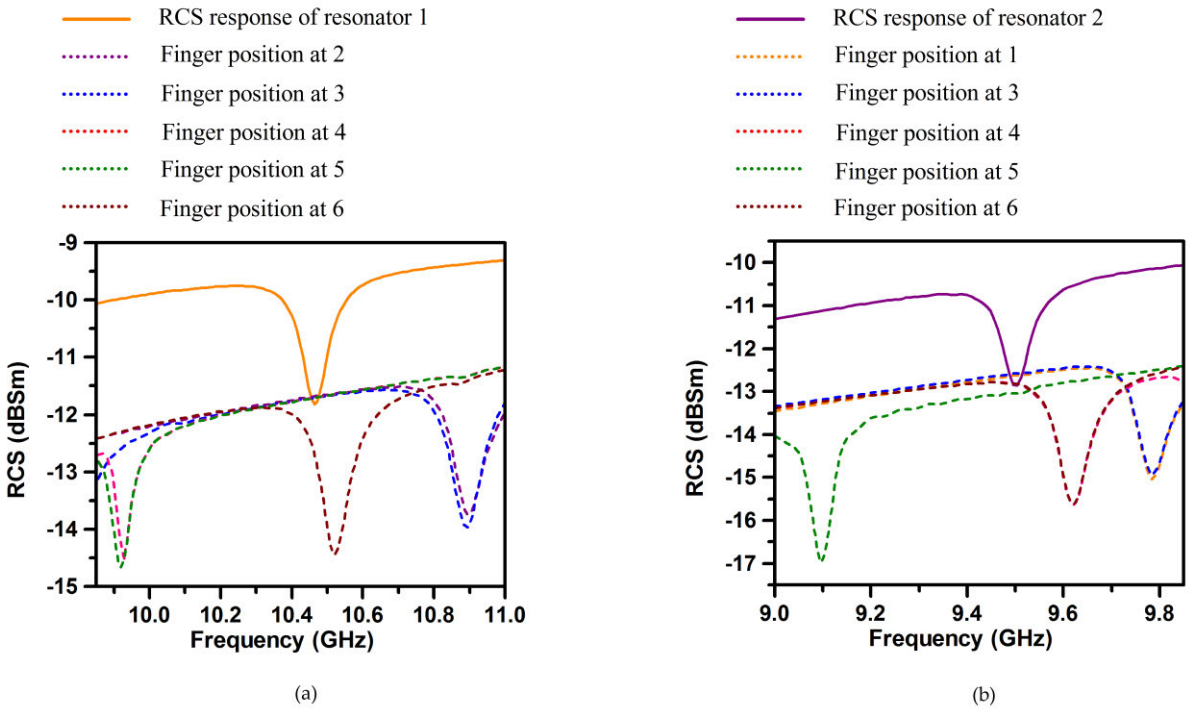

FIGURE 12. Solid line represents computed RCS response for the untouched states of the resonators (a) 1, (b) 2. Dotted lines exhibit the same resonator's response for human digit position on nearby resonators with color scheme 1, 2, 3, 4, 5, 6.

the ground effect the intelligibility of the encoded information slightly. The phenomenon becomes pronounced at smaller distances between the chipless RFID sensor and the floor and becomes less of a concern at larger distances. In practical settings, the proposed sensor will be placed at a height roughly equal to two-thirds of an average human. Placement of the sensor-incorporated tag at such distances from the ground would, in most cases, ensure that the reflections taking place from the floor's surface have little to no effect on the integrity and intelligibility of information encoded in the RCS response of the sensor incorporated tag.

In order to ensure that both touch detection and localization function seamlessly, the spectral bounds designated to each resonant element must not overlap with each other despite existence of coupling effects that exists between different resonant elements. The spectral bandwidth set to be allocated to each resonant element has been determined using rigorous parametric optimization. Consider the first resonant, labelled 1 resonating at a value of 10.49 GHz in the untouched state. Upon coming in direct contact with human digit, the spectral dip associated with 1 undergoes a drastic shift due to a corresponding increase in the effective permittivity because of the fingertip coming in contact with the sensor itself. The contact causes the otherwise recognizable resonant dip present in its allocated spectral band to disappear and transgress well outside the band of interest, shifting towards a much-lowered end of the electromagnetic spectrum.

While coming in direct contact with a human digit has a visibly pronounced effect, it is also worth noting the electromagnetic response of a resonant structure is affected by touch events taking place in its vicinity. In essence, coupling that exists between various resonant elements also needs to be accounted for during the design and optimization phase. The dimensions of each resonant element as well as the spacing between the same plays a crucial role in determining the performance of the proposed sensor in terms of accuracy and reliability. The core motivation for having a distinct spectral band allocated to each of the resonant elements is to ensure that all possible combinations of touch events taking place at the resonant element itself, as well as in the surroundings, are accounted for in their entirety. Each resonant element has been analyzed individually, and the obtained results have been scrutinized for determination of appropriate spectral neighborhood for each resonant element. Fig. 12 presents the RCS response obtained for two resonant elements. In Fig. 12 (a), results for resonator 1 are presented. It can be clearly seen that while the resonant element does furnish an RCS response at 10.49 GHz in the untouched state, the resonant dip also undergoes a drift when a touch event takes place in its vicinity. And finally, the corresponding dip transcends beyond the assigned range when a touch event takes place at resonator 1, resulting in a pronounced absence which is readily observable. Taking into account the maximum and minimum values that the said resonant dip has been found to drift towards on either side of the touched state, a spectral band ranging from 9.85 GHz to 11 GHz.

TABLE 3. Comparison with the existing work.

	[30]	[31]	[32]	[33]	[34]	Proposed
Conductive material	Metallized paper	Silver nano-particle ink	Copper	Copper	Adhesive conductive fabric	Copper
Number of touch points	10	2	5	2	4	6
Untouched state	30-55 pF	1.83 GHz, 0.94 GHz	5170 MHz, 5305 MHz, 5515 MHz, 5665 MHz and 5800 MHz	2.75 GHz and 3.80 GHz	<1.91 GHz	4.98 GHz, 5.92 GHz, 6.86 GHz, 8.15 GHz, 9.50 GHz and 10.47 GHz
Touched state	1000-3000 pF	1.55 GHz, 0.81 GHz	6 dB-9.5 dB of filter gain change on the resonating frequency	2.55 GHz and 3.70 GHz	Frequency Shift 1.91 GHz-2.96 GHz	Disappearance of the particular resonant frequency
Category	Arduino based system	Microstrip-line based tag	Chipless tag+Antenna	RF-based using Split Ring Resonators	Chipless tag	Chipless tag
Fabrication method	Chemical etching	Ink jet printing	Conventional	Conventional	Adhesive conductive Fabric	Conventional
Fabrication complexity	High	High	Low	Low	High	Low
Robustness	High	High	High	High	Medium	High
Relative cost	High	High	High	Low	Low	Low

Similarly, in Fig. 12 (b), resonant element 2 generates an RCS dip at 9.46 GHz in the in the untouched state. The dip undergoes a significant shift along the spectral upon occurrence of touch events in the neighborhood of the resonant element. In the touched state, the spectral dip corresponding to the resonant element is nowhere to found within the allocated spectral band. Keeping in view the maximum and minimum drift towards either side, band starting from 9 GHz and extending to 9.85 GHz has been allocated to resonator 2 as the spectral neighborhood for the corresponding resonant peak.

Similar analysis is performed for resonant elements 3 through 6, and results obtained have been plotted in Fig. 13 (a) through Fig. 13 (d). For each of the resonators, the RCS response in the touched state is drawn using a solid line, whereas the same RCS response with a touch event taking place in the vicinity of the resonator is represented using a dotted line. It can be readily observed that the designated bands, that are assigned based on the maximum and minimum transgression of the resonant peaks for each resonant element, do not overlap with another. The arrangement ensures that there are no instances where false-positive detection of a touch event takes place.

A. SECURITY CODE RECOGNITION

Most modern-day communication devices are equipped with a pass key in the form of a security code. The code prevents unauthorized use of the device and is also used to thwart potential attempts at gaining access to personal data stored on-board the device. Moreover, there are also examples where access to a facility is secured by means of a security code that is required to be provided by the user before he or she can be allowed to enter premises. The proposed sensor-incorporated chipless RFID tag can readily be used for security code recognition applications whereby selective control over physical access to a sensitive facility or installation can be achieved. A security code made up of six digits at max can be registered and, at a later point in time, recognized using the proposed chipless touch sensor. The application is demonstrated with a use-case whereby a two-digit security code "36" is registered and recognized at a later point in time. Fig. 14 depicts the arrangement highlighting two resonant elements, namely resonator 3 and resonator 6, where the human digit is placed one after the another for security code registration and recognition. At time instance t_1, the human finger comes in contact with resonant element 3. This leads to the corresponding resonant dip previously observable at 8 GHz in the RCS response to disappear. As an outcome, the allocated spectral band (7.6 GHz to 8.8 GHz) has been left all without a resonant dip. At point t_2, the human digit is placed on resonator 6, resulting in the resonant peak positioned at 5 GHz residing in the band from 4.5 GHz to 5.3 GHz to disappear. Keeping track of how resonant peaks disappear over shorter consecutive instances of time allows

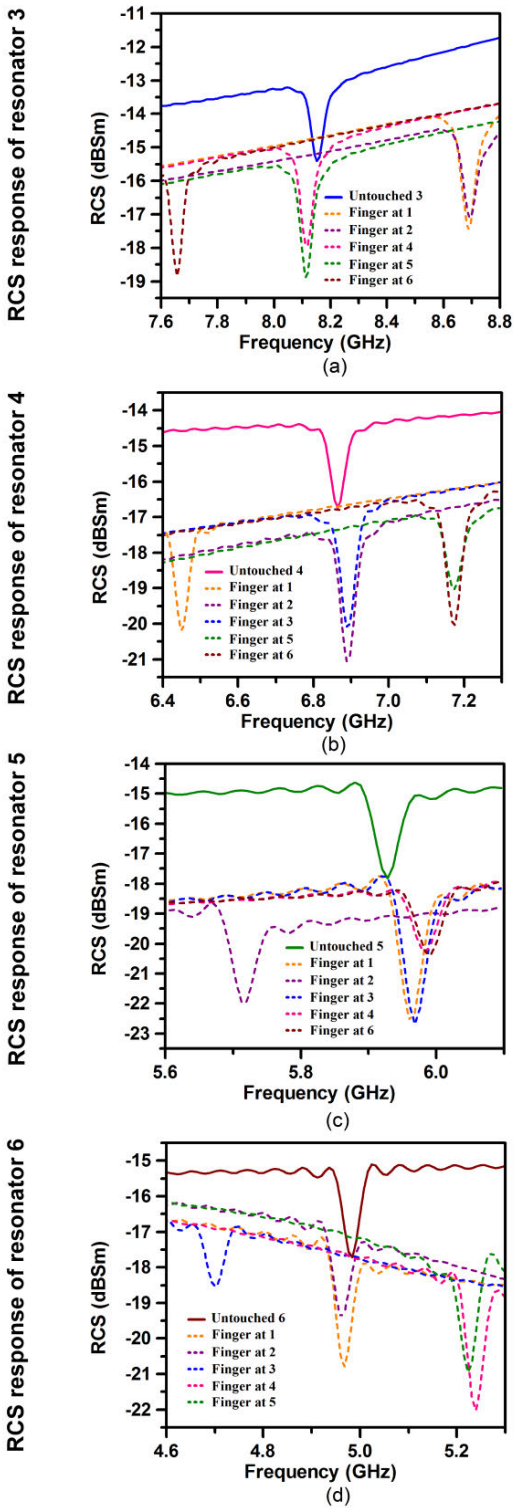

FIGURE 13. Solid line signifies computed RCS response for the untouched mode of the resonators (a) 3, (b) 4, (c) 5, (d) 6. Dotted lines exhibit the same resonator's response for human digit spot on neighboring resonators with color scheme 1, 2, 3, 4, 5, 6.

for setting up algorithms for registration and recognition of security codes.

Several prototypes of the proposed tag have been fabricated and are evaluated for their electromagnetic performance.

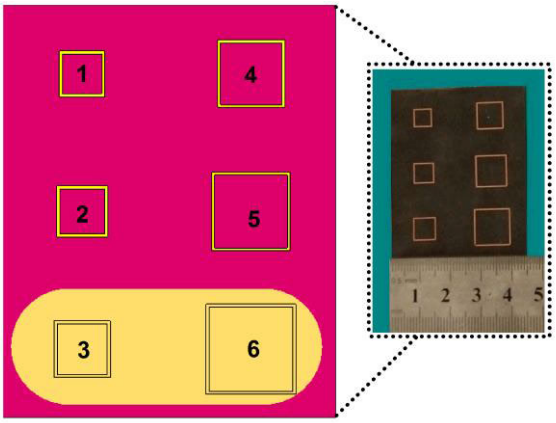

FIGURE 14. Evaluated swipe pattern and fabricated prototype.

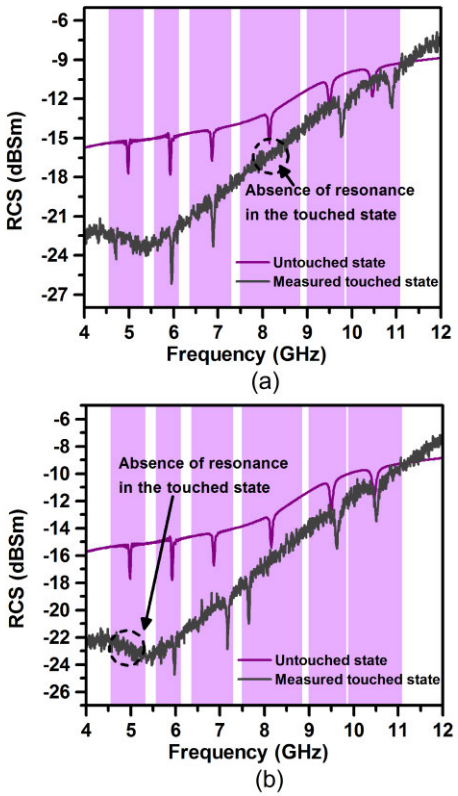

FIGURE 15. Experimental results affirming localization at (a) resonator 3 (b) resonator 6.

The experimental procedure for measuring the RCS is the same as explained earlier and draws heavily from the approach reported in [29]. The setup for recording the measurements comprises of two identical horn antennae, vector network analyzer (VNA) R&S® ZVL-13® and multiple prototypes under test. The measured results that have been obtained are coplotted with their computationally obtained counterparts for the purpose of comparison. From Fig. 15(a) & (b), it is evident that the measured results and the simulated findings are consistent with another, validating the functionality of the proposed sensor for detection and

localization of touch events. In the untouched state, it can be clearly seen that all six constituent elements resonate within their allocated spectral band along the spectral axes. As soon as a single touch-event takes place, the corresponding resonant peak disappears, and the overall count reduces to five instead of six. A quick inspection of the designated spectral bands reveals the exact location where the human digit has landed on the sensor which, in Fig. 11(a) is at resonator 3 and in 11(b) is resonator 6.

B. COMPARISON WITH THE EXISTING RESEARCH

The proposed chipless touch sensor is compared with state-of-the-art reported in literature Multiple techniques have been utilized in developing touchpads capable of sensing touch based on different physical parameters. Comparison of the proposed research work has been made with the published research and has been tabulated in Table 3.

IV. CONCLUSION

Implementation of chipless RFID tag as a touch sensor is put forward in this paper. Framed in a cautious manner, square resonators are capable of sensing touch; spotting location and lock codes as touch performance of every button is analyzed separately. Fabricated in a conventional manner and use of chipless technology offers a cost-effective solution in comparison to previous work. Its compactness makes it completely printable facilitating future implementation of the proposed design on organic substrates. The sensor holds potential for deployment in wearable smart cities and connected home sensors for user authentication and access control scenarios.

ACKNOWLEDGMENT

The authors pay wholeheartedly thanks to University of Engineering and Technology, Taxila for ACTSENA research funding. Gratitude is extended to National Institute of Electronics, Islamabad for extensive support during the prototype fabrication process.

REFERENCES

[1] F. Deng, Y. He, B. Li, Y. Song, and X. Wu, "Design of a slotted chipless RFID humidity sensor tag," *Sens. Actuators B Chem.*, vol. 264, pp. 255–262, Jul. 2018, doi: 10.1016/j.snb.2018.02.153.

[2] A. Zahra, H. Shahid, M. A. Riaz, Y. Amin, and H. Tenhunen, "A chipless RFID tag for smart temporal applications," *Int. J. RF Microw. Comput. Aided Eng.*, vol. 28, no. 8, Apr. 2018, Art. no. e21405, doi: 10.1002/mmce.21405.

[3] Y. Feng, L. Xie, Q. Chen, and L. Zheng, "Low-cost printed chipless RFID humidity sensor tag for intelligent packaging," *IEEE Sensors J.*, vol. 15, no. 6, pp. 3201–3208, Jun. 2015, doi: 10.1109/JSEN.2014.2385154.

[4] M. Borgese, F. A. Dicandia, F. Costa, S. Genovesi, and G. Manara, "An inkjet printed chipless RFID sensor for wireless humidity monitoring," *IEEE Sensors J.*, vol. 17, no. 15, pp. 4699–4707, Aug. 2017, doi: 10.1109/JSEN.2017.2712190.

[5] M. Borgese, F. A. Dicandia, F. Costa, S. Genovesi, and G. Manara, "Exploitation of chipless RFID technology for humidity monitoring," in *Proc. 32nd Gen. Assem. Sci. Symp. Int. Union Radio Sci. (URSI GASS)*, Montreal, QC, Canada, Aug. 2017, pp. 1–4, doi: 10.23919/URSIGASS.2017.8104972.

[6] S. Zeb, A. Habib, J. A. Satti, Y. Amin, J. Loo, and H. Tenhunen, "Dual-polarized chipless humidity sensor tag," *IEICE Electron. Express*, vol. 14, no. 21, Oct. 2017, Art. no. 20170926, doi: 10.1587/elex.14.20170926.

[7] C. Gaspar, J. Olkkonen, S. Passoja, and M. Smolander, "Paper as active layer in inkjet-printed capacitive humidity sensors," *Sensors*, vol. 17, no. 7, p. 1464, Jun. 2017, doi: 10.3390/s17071464.

[8] H. Andersson, A. Manuilskiy, T. Unander, C. Lidenmark, S. Forsberg, and H.-E. Nilsson, "Inkjet printed silver nanoparticle humidity sensor with memory effect on paper," *IEEE Sensors J.*, vol. 12, no. 6, pp. 1901–1905, Jun. 2012, doi: 10.1109/JSEN.2011.2182044.

[9] J. A. Satti, A. Habib, H. Anam, S. Zeb, Y. Amin, J. Loo, and H. Tenhunen, "Miniaturized humidity and temperature sensing RFID enabled tags," *Int. J. RF Microw. Comput.-Aided Eng.*, vol. 28, no. 1, Jan. 2018, Art. no. e21151, doi: 10.1002/mmce.21151.

[10] T. Noor, A. Habib, Y. Amin, J. Loo, and H. Tenhunen, "High-density chipless RFID tag for temperature sensing," *Electron. Lett.*, vol. 52, no. 8, pp. 620–622, Mar. 2016, doi: 10.1049/el.2015.4488.

[11] H. E. Matbouly, K. Zannas, Y. Duroc, and S. Tedjini, "Chipless wireless temperature sensor based on C-like scatterer for standard RFID reader," in *Proc. 32nd Gen. Assem. Sci. Symp. Int. Union Radio Sci. (URSI GASS)*, Montreal, QC, Canada, Aug. 2017, pp. 1–3, doi: 10.23919/URSIGASS.2017.8105026.

[12] H. E. Matbouly, S. Tedjini, K. Zannas, and Y. Duroc, "Compact multi bit slotted C-scatterer for threshold sensitive chipless wireless temperature sensor," *Technologies*, vol. 6, no. 3, p. 59, Jun. 201, doi: 10.3390/technologies6030059.

[13] A. Vena, L. Sydänheimo, M. M. Tentzeris, and L. Ukkonen, "A novel inkjet printed carbon nanotube-based chipless RFID sensor for gas detection," in *Proc. Eur. Microw. Conf.*, Nuremberg, Germany, 2013, pp. 9–12, doi: 10.23919/EuMC.2013.6686577.

[14] B. S. Cook, R. Vyas, S. Kim, T. Thai, T. Le, A. Traille, H. Aubert, and M. M. Tentzeris, "RFID-based sensors for zero-power autonomous wireless sensor networks," *IEEE Sensors J.*, vol. 14, no. 8, pp. 2419–2431, Aug. 2014, doi: 10.1109/JSEN.2013.2297436.

[15] S. Kim, Y. Kawahara, A. Georgiadis, A. Collado, and M. M. Tentzeris, "Low-cost inkjet-printed fully passive RFID tags using metamaterial-inspired antennas for capacitive sensing applications," in *IEEE MTT-S Int. Microw. Symp. Dig.*, Seattle, WA, USA, Jun. 2013, pp. 1–4, doi: 10.1109/MWSYM.2013.6697644.

[16] B. Andò, S. Baglio, V. Marletta, and A. Pistorio, "A contactless inkjet printed passive touch sensor," in *Proc. IEEE Int. Instrum. Meas. Technol. Conf. (I2MTC)*, Montevideo, Uruguay, May 2014, pp. 1638–1642, doi: 10.1109/I2MTC.2014.6861023.

[17] A. P. Sample, D. J. Yeager, and J. R. Smith, "A capacitive touch interface for passive RFID tags," in *Proc. IEEE Int. Conf. RFID*, Orlando, FL, USA, Apr. 2009, pp. 103–109, doi: 10.1109/RFID.2009.4911212.

[18] F. Costa, S. Genovesi, and A. Monorchio, "A chipless RFID based on multiresonant high-impedance surfaces," *IEEE Trans. Microw. Theory Techn.*, vol. 61, no. 1, pp. 146–153, Jan. 2013, doi: 10.1109/TMTT.2012.2227777.

[19] N. Barbot and E. Perret, "Gesture recognition with the chipless RIFD technology," in *Proc. 32nd Gen. Assem. Sci. Symp. Int. Union Radio Sci. (URSI GASS)*, Montreal, QC, Canada, Aug. 2017, pp. 1–3, doi: 10.23919/URSIGASS.2017.8104990.

[20] N. Javed, A. Habib, A. Akram, Y. Amin, and H. Tenhunen, "16-bit frequency signatured directly printable tag for organic electronics," *IEICE Electron. Express*, vol. 13, no. 11, May 2016, Art. no. 20160406, doi: 10.1587/elex.13.20160406.

[21] H. Anam, A. Habib, S. I. Jafri, Y. Amin, and H. Tenhunen, "Directly printable frequency signatured chipless RFID tag for IoT applications," *Radioengineering*, vol. 26, no. 1, pp. 139–146, Apr. 2017, doi: 10.13164/re.2017.0139.

[22] M. A. Riaz, Y. Abdullah, H. Shahid, Y. Amin, A. Akram, and H. Tenhunen, "Novel butterfly slot based chipless RFID tag," *Radioengineering*, vol. 27, no. 3, p. 777, Sep. 2018, doi: 10.13164/re.2018.0776.

[23] Adaptivity and Layout-General Layout Considerations. *IOS-Visual Design—Human Interface Guidelines—Apple Developer*. Accessed: Aug. 1, 2019. [Online]. Available: https://developer.apple.com/design/human-interface-guidelines/ios/visual-design/adaptivity-and-layout/

[24] Touch Target Size. *Android Accessibility Help*. Accessed: Aug. 1, 2019. [Online]. Available: https://support.google.com/accessibility/android/answer/7101858?hl=en

[25] B. Aslam, U. H. Khan, M. A. Azam, Y. Amin, J. Loo, and H. Tenhunen, "Miniaturized decoupled slotted patch RFID tag antennas for wearable health care," *Int. J. RF Microw. Comput.-Aided Eng.*, vol. 27, no. 1, Jan. 2017, Art. no. e21048, doi: 10.1002/mmce.21048.

[26] M. Darowish, R. Brenneman, and J. Bigger, "Dimensional analysis of the distal phalanx with consideration of distal interphalangeal joint arthrodesis using a headless compression screw," *Hand*, vol. 10, no. 1, pp. 100–104, Mar. 2015, doi: 10.1007/s11552-014-9679-x.
[27] Medical Illustration-Finger Anatomy. *MedicineNet*. Accessed: Aug. 1, 2019. [Online]. Available: https://www.medicinenet.com/image-collection/finger_anatomy_picture/picture.htm
[28] K. Dandekar, B. I. Raju, and M. A. Srinivasan, "3-D finite-element models of human and monkey fingertips to investigate the mechanics of tactile sense," *J. Biomech. Eng.*, vol. 125, no. 5, pp. 682–691, Oct. 2003, doi: 10.1115/1.1613673.
[29] A. Vena, E. Perret, and S. Tedjini, "Chipless RFID tag using hybrid coding technique," *IEEE Trans. Microw. Theory Techn.*, vol. 59, no. 12, pp. 3356–3364, Dec. 2011, doi: 10.1109/tmtt.2011.2171001.
[30] A. D. Mazzeo, W. B. Kalb, L. Chan, M. G. Killian, J.-F. Bloch, B. A. Mazzeo, and G. M. Whitesides, "Paper-based, capacitive touch pads," *Adv. Mater.*, vol. 24, no. 21, pp. 2850–2856, Apr. 2012, doi: 10.1002/adma.201200137.
[31] S. Choi, S. Eom, M. M. Tentzeris, and S. Lim, "Inkjet-printed electromagnet-based touchpad using spiral resonators," *J. Microelectromech. Syst.*, vol. 25, no. 5, pp. 947–953, Oct. 2016, doi: 10.1109/JMEMS.2016.2593956.
[32] C. Gao, Y. Li, and X. Zhang, "LiveTag: Sensing human-object interaction through passive chipless WiFi tags," in *Proc. 15th USENIX Symp. Netw. Syst. Design Implement. (NSDI)*, Renton, WA, USA, Apr. 2018, pp. 533–546.
[33] M. U. Memon, H. Jeong, and S. Lim, "Metamaterial-inspired radio frequency based touchpad sensor system," *IEEE Trans. Instrum. Meas.*, to be published, doi: 10.1109/TIM.2019.2908507.
[34] L. Corchia, G. Monti, E. De Benedetto, and L. Tarricone, "Low-cost chipless sensor tags for wearable user interfaces," *IEEE Sensors J.*, vol. 19, no. 21, pp. 10046–10053, Nov. 2019, doi: 10.1109/JSEN.2019.2927823.

LAIBA SHAHID received the B.Sc. degree in telecommunication engineering from the University of Engineering and Technology, Taxila, in 2016, where she is currently pursuing the M.S. degree with the Telecommunication Department. Her research interests include RFID and chipless RFID sensor tags.

HUMAYUN SHAHID received the B.S. degree in communication systems engineering from the Institute of Space Technology, Islamabad, in 2008, and the M.S. degree in signal processing from Nanyang Technological University, Singapore, in 2011. He joined the Space and Upper Atmosphere Research Commission (SUPARCO), where he worked on radiation-hardened space grade components for telemetry subsystems. He joined the Department of Telecommunication Engineering, University of Engineering and Technology, Taxila, where he currently works as an Assistant Professor. He is also affiliated with the ACTSENA Research Group working toward design and signal processing related aspects of electromagnetic transduction-based sensor-incorporated chipless RFID tags. He is also the Director of the Departmental Antenna and the RF Laboratory. His research work has been featured in a number of ISI indexed journals and international conferences.

MUHAMMAD ALI RIAZ received the B.S. and M.S. degrees in electrical engineering from Iowa State University, USA, in 2009 and 2010, respectively, and the Ph.D. degree in telecommunication engineering from the University of Engineering and Technology, Taxila, Pakistan, in 2019. He joined the Department of Electrical and Computer Engineering, Iowa State University, as a Research Assistant. He is currently working as an Assistant Professor with the Telecommunication Engineering Department, University of Engineering and Technology. He is also involved in the design and implementation of chipless RFID tags, based on electromagnetic signature and their signal processing applications under the ACTSENA Research Group. He is also the Director of the Electronics and Measurements Laboratory, Department of Telecommunication Engineering. His research work has been featured in a number of international conferences and ISI-indexed journals.

SYEDA IFFAT NAQVI received the B.Sc.Eng. degree in computer engineering and the M.Sc. degree in telecommunication engineering from the University of Engineering and Technology, Taxila, Pakistan, in 2006 and 2011, respectively. She is currently serving as an Assistant Professor and also associated with the ACTSENA Research Group, University of Engineering and Technology. She is also working toward the design and implementation of multiple antenna array systems for current 4G and next generation millimeter-wave 5G mobile communication applications. She has authored or coauthored numerous technical articles in ISI-indexed journals and international conferences.

MUHAMMAD JAMIL KHAN received the B.Sc.Eng. degree in computer engineering, the M.Sc. degree in telecommunication engineering, and the Ph.D. degree in computer engineering from the University of Engineering and Technology, Taxila, Pakistan, in 2005, 2009, and 2016, respectively. He is currently an Assistant Professor and the Director of the Embedded Systems and Digital Signal Processing Laboratory, University of Engineering and Technology, where he is also the Founder of the Virtual Reality Simulation Laboratory. He has authored or coauthored numerous technical articles in well-known international journals and conferences. His current research interests include multimedia content analysis, RF identification, and machine learning.

MANSOOR SHAUKAT KHAN received the degree from PU Lahore, Pakistan, in 1994, the M.Sc. degree in statistics from the University of ARID Agriculture Rawalpindi, Pakistan, in 2000, and the Ph.D. degree from the Beijing Institute of Technology (BIT), China, in January 2016. He is currently working as an Assistant Professor with the Department of Mathematics, COMSATS University Islamabad, Pakistan. He has more than ten research articles in reputed journals and proceedings of international conferences. His research interests include mathematical modeling and optimization, quality and reliability engineering, survival analysis, spatial data analysis, and data science. He received the National Research Program for Universities Award from HEC Pakistan.

YASAR AMIN received the B.Sc. degree in electrical engineering with specialization in telecommunication and the M.B.A. degree in innovation and growth from the Turku School of Economics, University of Turku, Finland, the M.Sc. degree in electrical engineering with specialization in system on chip design and the Ph.D. degree in electronic and computer systems from the Royal Institute of Technology (KTH), Sweden, with the research focuses on printable green RFID antennas for embedded sensors. He is currently an Associate Professor and the Chairman of Telecommunication Engineering Department, University of Engineering and Technology, Taxila, Pakistan. He also serves as the Director of the Embedded Systems Research and Development Centre. He is also the Founder of the Agile Creative Technologies for Smart Electromagnetic Novel Applications (ACTSENA) Research Group. He has authored or coauthored more than 100 international technical articles in conferences and journals. His research interests include the design and application of multiple antenna systems for next-generation mobile communication systems, millimeter-wave and terahertz antenna array, implantable and wearable electronics, and inkjet printing technology in microwave applications. He is a member of more than a dozen international professional societies and a Fellow of PAE.

JONATHAN LOO (KOK-KEONG LOO) received the M.Sc. degree in electronics and the Ph.D. degree in electronics and communications from the University of Hertfordshire, U.K., in 1998 and 2003, respectively. He leads a Research Team of eight Ph.D. degree students in the area of communication and networking. He is currently a Professor and the Chair of computing and communication engineering with the School of Computing and Engineering, University of West London, U.K. His research interest includes network architecture, communication protocols, network security, embedded systems, video coding and transmission, wireless communications, digital signal processing, and optical networks. He has successfully graduated 13 Ph.D. degrees as a Principle Supervisor and contributed over 175 publications in the aforementioned specialist areas.